CONF-930404--10

To be Presented at Joint International Conference on Mathematical Methods and Supercomputing in Nuclear Applications, Karlsruhe, Germany, April 19-23, 1993

Direct Solution of the Mathematical Adjoint Equations for an Interface Current Nodal Formulation

ANL/RA/CP--76759

DE93 009961

T. A. Taiwo, W. S. Yang, and H. S. Khalil
Reactor Analysis Division

Argonne National Laboratory
9700 South Cass Avenue
Argonne, IL 60439
(708) 252-5621

* Work supported by the U.S. Department of Energy, Nuclear Energy Programs under Contract W-31-109-ENG-38.

DIRECT SOLUTION OF THE MATHEMATICAL ADJOINT EQUATIONS FOR AN INTERFACE CURRENT NODAL FORMULATION

T. A. Taiwo, W. S. Yang, H. S. Khalil
Reactor Analysis Division
Argonne National Laboratory
Argonne, Illinois 60439, U.S.A.

ABSTRACT

A numerical method for directly computing the mathematical adjoint flux moments and partial currents for the hexagonal-Z geometry interface current nodal formulation in the DIF3D code is described. The new scheme is developed as an alternative to an existing scheme that employs a similarity transformation of the physical adjoint solution to compute the mathematical adjoint. Whereas the existing scheme is rigorous only when the flat transverse-leakage approximation is employed, this new scheme is exact for all leakage approximations in the DIF3D nodal method. In the new scheme, adjoint nodal equations whose form is very similar to that of the forward nodal equations are derived by employing linear combinations of the adjoint partial currents as computational unknowns in the adjoint equations. This enables the use of the forward solution algorithm with only minor modifications for solving the mathematical adjoint equations. By using the new scheme as a reference method, it is shown numerically that while the results computed with the existing scheme are approximate, they are sufficiently accurate for calculations of global and local reactivity changes resulting from coolant voiding in a liquid metal reactor.

INTRODUCTION

The application of advanced nodal methods in perturbation theory calculations and kinetics calculations based on space-time factorization schemes requires the solution of the mathematical adjoint nodal equations.[1-4] For each nodal scheme, the *mathematical* adjoint equations are obtained by transposing the global matrix associated with the nodal unknowns.

The direct solution of the mathematical adjoint equations for the analytical nodal method embodied in the QUANDRY code was described in reference 5. For the interface current scheme used in the nodal option of the DIF3D code,[6] an approximate solution of the mathematical adjoint equations, obtained via an intermediate solution (the so called physical adjoint) and a similarity transformation, has been given by Lawrence[1] and more recently by Yang.[7] The *physical* adjoint is obtained by applying the nodal differencing approach to the equation adjoint to the *spatially continuous* multigroup diffusion equation and is generally different from the mathematical adjoint.

The similarity transformation approach has been in routine use for obtaining the DIF3D-nodal adjoint. This approach is exact for two-dimensional hexagonal geometry problems as a consequence of the particular approximation made in representing the spatial shape of the leakage transverse to each of the hex-plane coordinate directions.[6] For three-dimensional hexagonal-Z problems, however, the transformation is exact only when the flat transverse-leakage approximation is used. When the quadratic transverse-leakage approximation is employed, the similarity transformation approach gives the exact mathematical adjoint only in the limit of zero axial mesh spacing[1,7] (in which case the approximation is equivalent to the flat transverse-leakage approximation).

In this paper, we describe a direct and thus rigorous scheme for the solution of the DIF3D-nodal mathematical adjoint equations. We first derive the mathematical adjoint nodal equations and show how these equations can be cast in a form very similar to that of the forward nodal equations. We then describe the iterative numerical approach used to solve the adjoint equations. Finally, we present numerical results illustrating the differences in perturbation theory predictions of local and global reactivity changes obtained using the new (direct) solution approach and the previous, approximate scheme involving a similarity transformation.

DERIVATION AND SOLUTION OF THE MATHEMATICAL ADJOINT EQUATIONS

DIF3D Nodal Formulation and Notation

The DIF3D-nodal scheme employs a nodal expansion method (NEM) and the interface current formulation for solving the multigroup neutron diffusion equation. In the forward solution approach, equations for the nodal unknowns are derived and solved along with specified external boundary conditions and the requirement that the interface partial currents be continuous.[6] In hexagonal-Z geometry problems, the nodal unknowns are five flux moments and eight interface partial currents. For a given neutron energy group g, the nodal equations for these unknowns are written simultaneously for all nodes as follows:

$$v\left[S_g\phi_{gh} + T_g J^o_{gh} - Y_g J^{in}_{gh} + W_g\left(J^o_{gz} - J^{in}_{gz}\right)\right] = vQ_{gh}\,, \tag{1}$$

$$v_z\left[S_{gz}\phi_{gz} + U_g J^o_{gz} - V_g J^{in}_{gz} + H_g\left(J^o_{gh} - J^{in}_{gh}\right)\right] = v_z Q_{gz}\,, \tag{2}$$

$$n\left[-B_g\phi_{gh} + J^o_{gh} - C_g J^{in}_{gh}\right] = 0\,, \tag{3}$$

$$n_z\left[-N_g\phi_{gh} - M_g\phi_{gz} + J^o_{gz} - F_g J^{in}_{gz}\right] = 0\,, \tag{4}$$

$$n\left[-\Pi J^o_{gh} + J^{in}_{gh}\right] = 0\,, \tag{5}$$

$$n_z\left[-\Pi_z J^o_{gz} + J^{in}_{gz}\right] = 0\,, \tag{6}$$

where

ϕ_{gh} is a vector containing the node-averaged flux (zeroth flux moment) and hexagonal-plane flux moments for all nodes,

ϕ_{gz} is a vector containing the axial-direction flux moments for all nodes,

J^o_{gh} and J^{in}_{gh} are vectors containing the hex-plane outgoing and incoming interface partial currents, respectively, for all nodes,

J^o_{gz} and J^{in}_{gz} are vectors containing the axial-direction outgoing and incoming interface partial currents, respectively, for all nodes,

Q_{gh} is a vector containing the node-averaged and hex-plane source moments,

Q_{gz} is a vector containing the axial-direction source moments,

$\boldsymbol{v}$ is a block-diagonal matrix containing the nodal volumes, with each (4x4) diagonal block having only diagonal elements equal to the nodal volume ($\sqrt{3}h^2\Delta z^k/2$, where $h \equiv$ lattice pitch , and $\Delta z^k \equiv$ node-k axial dimension),

$\boldsymbol{v}_z$ is a diagonal matrix containing nodal volumes,

$\boldsymbol{n}$ is a block-diagonal matrix, with each (6x6) diagonal block having only diagonal elements equal to the nodal surface area $(h\Delta z^k/\sqrt{3})$ normal to a hex-plane coordinate direction,

$\boldsymbol{n}_z$ is a diagonal matrix containing the nodal surface area $(\sqrt{3}h^2/2)$ normal to the Z-direction.

The elements of the matrices $\boldsymbol{S}_g$ and $\boldsymbol{S}_{gz}$ depend on the removal cross sections, diffusion coefficients, and the lattice pitch. The matrices $\boldsymbol{T}_g$, $\boldsymbol{Y}_g$, $\boldsymbol{W}_g$, $\boldsymbol{U}_g$, $\boldsymbol{V}_g$, $\boldsymbol{H}_g$, $\boldsymbol{B}_g$, $\boldsymbol{C}_g$, $\boldsymbol{N}_g$, $\boldsymbol{M}_g$, and $\boldsymbol{F}_g$, are coupling coefficient matrices defined in terms of the diffusion coefficients, the lattice pitch, and axial mesh sizes. All these matrices are block-diagonal with the exception of $\boldsymbol{H}_g$ which is block-tridiagonal. The $\boldsymbol{H}_g$ matrix, which arises in the nodal equations because of the quadratic fit used to represent the leakage transverse to the axial direction, couples the fluxes of a node to the partial currents of the node and the neighboring axial nodes. The matrices Π and Π_z are symmetric; they contain a single non-zero element in each row with a value of either one (expressing continuity of partial currents across internal surfaces), or an albedo constant (expressing the fixed ratio specified by conditions at an outer boundary). The nodal volume and surface matrices $\boldsymbol{v}$, $\boldsymbol{v}_z$, $\boldsymbol{n}$, and $\boldsymbol{n}_z$ are retained in Eqs. (1) to (6) to express neutron balance in the same form typically applied in nodal perturbation theory expressions.

For group g, the response matrix equation solved iteratively by the DIF3D code is obtained by using Eqs. (1) and (2) to eliminate the flux moments from Eqs. (3) and (4). The resulting

response matrix equation can be written in the form

$$J_g^o = \hat{P}_g \{Q_g - \hat{L}_g\} + \hat{R}_g J_g^{in} , \tag{7}$$

where

$$\hat{P}_g = \hat{A}_g^{-1} \hat{B}_g , \tag{8}$$

$$\hat{R}_g = \hat{A}_g^{-1} \hat{C}_g , \tag{9}$$

$$\hat{A}_g = \begin{bmatrix} [I + B_g S_g^{-1} T_g] & [B_g S_g^{-1} W_g] \\ [N_g S_g^{-1} T_g] & [I + M_g S_{gz}^{-1} U_g + N_g S_g^{-1} W_g] \end{bmatrix}, \tag{10}$$

$$\hat{B}_g = \begin{bmatrix} [B_g S_g^{-1}] & [0] \\ [N_g S_g^{-1}] & [M_g S_{gz}^{-1}] \end{bmatrix}, \tag{11}$$

$$\hat{C}_g = \begin{bmatrix} [C_g + B_g S_g^{-1} Y_g] & [B_g S_g^{-1} W_g] \\ [N_g S_g^{-1} Y_g] & [F_g + M_g S_{gz}^{-1} V_g + N_g S_g^{-1} W_g] \end{bmatrix}, \tag{12}$$

$$J_g^r = col \left[J_{gh}^r , J_{gz}^r \right], \qquad r = o, \text{ or } in, \tag{13}$$

$$Q_g = col \ [Q_{gh}, Q_{gz}] , \tag{14}$$

$$\hat{L}_g = col \ [0, L_g] , \tag{15}$$

and where the transverse leakage L_g is given by

$$L_g = H_g (J_{gh}^o - J_{gh}^{in}) . \tag{16}$$

Because the matrices $\hat{P}_g$ and $\hat{R}_g$ are block-diagonal, Eq. (7) relates the eight outgoing partial currents from each node to the eight incoming partial currents, and to the source and transverse leakage terms for the node. The transverse leakage term, which appears only in the axial direction partial current equations, depends on the hex-plane (incoming and outgoing) partial currents for the node in question and the two adjacent axial nodes.

In DIF3D-nodal, Eq. (7) is solved numerically (inner iteration) along with Eqs. (1) and (2) during each outer (fission source) iteration. The outer iteration is accelerated by asymptotic source extrapolation and coarse-mesh rebalance (CMR).

Mathematical Adjoint Formulation

The mathematical adjoint is defined by the requirement that its use as the weight function in the nodal perturbation theory expression for reactivity eliminates first-order terms involving the perturbation in the vector of nodal unknowns. This requirement is satisfied if the mathematical adjoint vector Γ_0^* is the solution of the equation

$$\boldsymbol{h}_0^T \Gamma_0^* = 0 , \tag{17}$$

where $\boldsymbol{h}_0$ is the global matrix obtained by combining Eqs. (1) to (6) for all groups into the form

$$\boldsymbol{h}_0 \Gamma_0 = 0 , \tag{18}$$

and Γ_0 is a vector containing nodal flux moments and node-surface partial currents for all groups.

The group-g component of the mathematical adjoint equation (Eq. (17)) can be written as the following set of equations:

$$\boldsymbol{S}_g \boldsymbol{v} \phi_{gh}^* - \boldsymbol{B}_g^T \boldsymbol{n} J_{gh}^{o*} - \boldsymbol{N}_g^T \boldsymbol{n}_z J_{gz}^{o*} = \boldsymbol{v} Q_{gh}^* , \tag{19}$$

$$\boldsymbol{S}_{gz} \boldsymbol{v}_z \phi_{gz}^* - \boldsymbol{M}_g^T \boldsymbol{n}_z J_{gz}^{o*} = \boldsymbol{v}_z Q_{gz}^* , \tag{20}$$

$$\boldsymbol{T}_g^T \boldsymbol{v} \phi_{gh}^* + \boldsymbol{H}_g^T \boldsymbol{v}_z \phi_{gz}^* + \boldsymbol{n} J_{gh}^{o*} - \Pi \boldsymbol{n} J_{gh}^{in*} = 0 , \tag{21}$$

$$\boldsymbol{W}_g^T \boldsymbol{v} \phi_{gh}^* + \boldsymbol{U}_g^T \boldsymbol{v}_z \phi_{gz}^* + \boldsymbol{n}_z J_{gz}^{o*} - \Pi_z \boldsymbol{n}_z J_{gz}^{in*} = 0 , \tag{22}$$

$$\boldsymbol{n} J_{gh}^{in*} - \boldsymbol{Y}_g^T \boldsymbol{v} \phi_{gh}^* - \boldsymbol{H}_g^T \boldsymbol{v}_z \phi_{gz}^* - \boldsymbol{C}_g^T \boldsymbol{n} J_{gh}^{o*} = 0 , \tag{23}$$

$$\boldsymbol{n}_z J_{gz}^{in*} - \boldsymbol{W}_g^T \boldsymbol{v} \phi_{gh}^* - \boldsymbol{V}_g^T \boldsymbol{v}_z \phi_{gz}^* - \boldsymbol{F}_g^T \boldsymbol{n}_z J_{gz}^{o*} = 0 , \tag{24}$$

where, for node k,

$$Q_{gh}^{k*} = \sum_{g' \neq g}^{G} \Sigma_{g'g}^{s,k} \phi_{g'h}^{k*} + \sum_{g'=1}^{G} \chi_{g'}^{k} \frac{\nu}{\lambda} \Sigma_g^{f,k} \phi_{g'h}^{k*} , \tag{25}$$

$$Q_{gz}^{k*} = \sum_{g' \neq g}^{G} \Sigma_{g'g}^{s,k} \phi_{g'z}^{k*} + \sum_{g'=1}^{G} \chi_{g'}^{k} \frac{\nu}{\lambda} \Sigma_g^{f,k} \phi_{g'z}^{k*} . \tag{26}$$

The vectors ϕ_{gh}^*, ϕ_{gz}^*, J_{gh}^{o*}, J_{gh}^{in*}, J_{gz}^{o*}, and J_{gz}^{in*} are the mathematical adjoint counterparts of the vectors appearing in Eqs. (1) to (6). In writing Eqs. (19) to (24), we have used the fact that the

matrices S_g, S_{gz}, ν, ν_z, n, and n_z are symmetric.

Overview of Existing Solution Approach

The direct solution of Eqs. (19) to (24) is complicated by the unusual coupling between the mathematical adjoint unknowns. As an alternative to solving these equations directly, Lawrence formulated a similarity transformation procedure[1,7] and applied it to the determination of the required mathematical adjoint flux moments from the *physical adjoint* flux moments $\tilde{\phi}^*_{gh}$ and $\tilde{\phi}^*_{gz}$. The physical adjoint flux moments are computed by solving the spatially-continuous multigroup adjoint diffusion equations using the DIF3D-nodal approach. This is readily accomplished by appropriately redefining macroscopic cross section parameters (similar to the approach employed by finite difference codes[8]) and using the new parameters in the forward solution scheme. The matrix similarity transformation can be written as

$$\begin{bmatrix} \phi^*_{gh} \\ \phi^*_{gz} \end{bmatrix} = \begin{bmatrix} X_1 & 0 \\ 0 & X_2 \end{bmatrix} \begin{bmatrix} \tilde{\phi}^*_{gh} \\ \tilde{\phi}^*_{gz} \end{bmatrix} \equiv X \begin{bmatrix} \tilde{\phi}^*_{gh} \\ \tilde{\phi}^*_{gz} \end{bmatrix}, \tag{27}$$

where X is the similarity transformation matrix.[1,7] This similarity transformation approach is approximate for the general hexagonal-Z geometry case with the quadratic transverse-leakage approximation; it is exact only if the flat transverse-leakage approximation is employed or in the limit of zero axial mesh spacing.[1,7] This generally approximate scheme for computing the mathematical adjoint flux moments is the existing scheme in the DIF3D code.[6]

Following the calculation of the mathematical adjoint fluxes in the existing scheme, the mathematical adjoint partial currents are determined by solving the equations

$$nJ^{o*}_{gh} = \Pi C^T_g n J^{o*}_{gh} - (T^T_g - \Pi Y^T_g)\, \nu\phi^*_{gh} - (I - \Pi)\, H^T_g \nu_z \phi^*_{gz}, \tag{28}$$

and

$$n_z J^{o*}_{gz} = \Pi_z F^T_g n_z J^{o*}_{gz} - (I - \Pi_z)\, W^T_g \nu\phi^*_{gh} - (U^T_g - \Pi_z V^T_g)\, \nu_z \phi^*_{gz}, \tag{29}$$

where I is the identity matrix. These equations are obtained by using Eqs. (23) and (24) to eliminate the adjoint incoming partial currents from Eqs. (21) and (22). By reordering the unknown adjoint partial currents in Eqs. (28) and (29), these equations can be solved using the same iterative scheme employed for solving the forward response matrix equation (Eq. (7)) at each outer iteration. Finally, we note that if the flat transverse-leakage approximation is made, it is possible to derive simple expressions relating the mathematical adjoint partial currents to the physical adjoint partial currents and flux moments, thereby eliminating the need for iteration in solving Eqs. (28) and (29).

New Direct Solution Approach

Equations (19), (20), (28) and (29) constitute a rigorous set of equations for the unknown mathematical adjoint flux moments and partial currents. It would appear on the surface that these unknowns can be computed via a global solution strategy in which Eqs. (28) and (29) are solved (using the scheme described above with no further modifications) along with Eqs. (19) and (20). This approach would, however, result in an unconventional outer iteration of the form

$$\psi^{*(n)} = \frac{1}{\lambda^{(n-1)}} \boldsymbol{D}\psi^{*(n-1)} + \boldsymbol{E}\phi^{*(n-1)} , \tag{30}$$

$$\lambda^{(n)} = \lambda^{(n-1)} \frac{\langle 1 , \psi^{*(n)} \rangle}{\langle 1 , \psi^{*(n-1)} \rangle} , \tag{31}$$

where ψ^* is the adjoint fission source vector and, $\boldsymbol{D}$ and $\boldsymbol{E}$ are global matrices whose precise form need not be described here. Because Eqs. (30) and (31) differ from the conventional fission source iteration, their solution would require the development of a new global iteration strategy.

An alternative direct solution approach, requiring no major changes to the DIF3D nodal iteration strategy, was developed. This approach consisted of deriving response matrix equations for the adjoint partial currents in terms of the *adjoint source moments*; these equations are analogous to the corresponding response matrix equations in the forward scheme. This was accomplished by eliminating the adjoint flux moments from Eqs. (28) and (29) using Eqs. (19) and (20) to obtain

$$\hat{\boldsymbol{A}}_g^T J_g^{o*} = \tilde{\Pi}\hat{\boldsymbol{C}}_g^T J_g^{o*} + \hat{\boldsymbol{B}}_g^* Q_g^* - \boldsymbol{Z}_g J_g^{o*} , \tag{32}$$

where

$$J_g^{o*} = col\left[\boldsymbol{n}J_{gh}^{o*} , \boldsymbol{n}_z J_{gz}^{o*}\right] , \tag{33}$$

$$Q_g^* = col\left[\boldsymbol{v}Q_{gh}^* , \boldsymbol{v}_z Q_{gz}^*\right] , \tag{34}$$

$$\hat{\boldsymbol{B}}_g^* = -\begin{bmatrix} [\boldsymbol{T}_g^T - \Pi \boldsymbol{Y}_g^T]\boldsymbol{S}_g^{-1} & [\boldsymbol{I} - \Pi]\boldsymbol{H}_g^T \boldsymbol{S}_{gz}^{-1} \\ [\boldsymbol{I} - \Pi_z]\boldsymbol{W}_g^T \boldsymbol{S}_g^{-1} & [\boldsymbol{U}_g^T - \Pi_z \boldsymbol{V}_g^T]\boldsymbol{S}_{gz}^{-1} \end{bmatrix} , \tag{35}$$

$$\tilde{\Pi} = \begin{bmatrix} \Pi & 0 \\ 0 & \Pi_z \end{bmatrix} , \tag{36}$$

$$\boldsymbol{Z}_g = \begin{bmatrix} 0 & [\boldsymbol{I} - \Pi]\, \boldsymbol{H}_g^T \boldsymbol{S}_{gz}^{-1} \boldsymbol{M}_g^T \\ 0 & 0 \end{bmatrix}, \tag{37}$$

and where the matrices $\hat{\boldsymbol{A}}_g$ and $\hat{\boldsymbol{C}}_g$ are defined by Eqs. (10) and (12), respectively.

In Eq. (32), the coupling between the adjoint unknowns is more complicated than that between the unknowns in the forward equation (Eq. (7)). Consider the coupling between partial currents. In the forward equation the outgoing partial currents for a node are coupled with *eight* partial currents coming into the node from the surrounding eight nodes, and with transverse leakage terms involving contributions from the hex-plane partial currents in the node and the twenty surrounding nodes. However, in the adjoint equation (Eq. (32) premultiplied with the inverse of $\hat{\boldsymbol{A}}_g^T$), the outgoing partial currents are coupled to *all* the outgoing partial currents of the eight neighboring nodes (i.e. 64 outgoing partial currents), as well as to *adjoint transverse-leakage* terms (last term in Eq. (32)) with contributions from the Z-direction partial currents in the node and the twenty surrounding nodes. These *adjoint transverse-leakage* terms arise because of the quadratic fit used to approximate the transverse leakage in deriving the forward nodal equation. Furthermore, whereas the transverse leakage terms appear only in the *Z-direction* partial current equation in the forward equation (Eq. (7)), they appear only in the *hex-plane* partial current equation in the adjoint equation (as is evident from the structure of $\boldsymbol{Z}_g$ in Eq. (32)).

The added complexity of the coupling between the outgoing partial currents (relative to that in the forward equations) can be eliminated by linearly combining the partial currents into interface quantities (which we call "combined partial currents") whose coupling is the same as that of the partial currents in the forward equations. Defining the combined partial currents as

$$\tilde{\boldsymbol{K}}_g^{o*} \equiv \begin{bmatrix} \boldsymbol{K}_{gh}^{o*} \\ \boldsymbol{K}_{gz}^{o*} \end{bmatrix} \equiv \hat{\boldsymbol{C}}_g^T \boldsymbol{J}_g^{o*}, \tag{38}$$

and the corresponding combined incoming partial currents as

$$\tilde{\boldsymbol{K}}_g^{in*} \equiv \tilde{\Pi} \tilde{\boldsymbol{K}}_g^{o*}, \tag{39}$$

we can write Eq. (32) as

$$\hat{\boldsymbol{A}}_g^T (\hat{\boldsymbol{C}}_g^T)^{-1} \tilde{\boldsymbol{K}}_g^{o*} = \tilde{\boldsymbol{K}}_g^{in*} + \hat{\boldsymbol{B}}_g^* \boldsymbol{Q}_g^* - \boldsymbol{Z}_g (\hat{\boldsymbol{C}}_g^T)^{-1} \tilde{\boldsymbol{K}}_g^{o*}. \tag{40}$$

Premultiplying Eq. (40) by the matrix $\hat{\boldsymbol{C}}_g^T (\hat{\boldsymbol{A}}_g^T)^{-1}$ ($= \hat{\boldsymbol{R}}_g^T$, the transpose of the response matrix appearing in the forward equation (Eq. (7)), we obtain

$$\tilde{K}_g^{o*} = \hat{R}_g^T \tilde{K}_g^{in*} + \hat{P}_g^* Q_g^* - \hat{L}_g^* , \tag{41}$$

where

$$\hat{P}_g^* = \hat{R}_g^T \hat{B}_g^* , \tag{42}$$

and

$$\hat{L}_g^* = \hat{R}_g^T Z_g (\hat{C}_g^T)^{-1} \tilde{K}_g^{o*} . \tag{43}$$

The importance of the linear combination specified by Eqs. (38) and (39) is that while Eqs. (21) and (22) indicate that the adjoint nodal partial currents are not continuous (compare these equations to the continuity relations, Eqs. (5) and (6) of the forward scheme), the combined partial currents are continuous. As a result, it becomes possible to apply the solution scheme of the forward response matrix equations[6] to Eq. (41) with minimal modification. In particular, the coupling between the combined partial currents now has the same structure as that between the partial currents in the forward equation, and only the formulation of the source terms is fundamentally different. For a given node, Eq. (41) reflects the fact that the outgoing partial currents from the node are coupled to the adjoint (fission, and scattering) sources in the node and the surrounding twenty nodes; this differs from the coupling in the forward equation (Eq. (7)) in which the coupling is limited to the sources for the node in question. Although additional code logic is required to compute the adjoint source and leakage terms, the new structure of these source terms causes no difficulty in applying the existing solution algorithm.

In the direct mathematical adjoint algorithm, Eq. (41) is used to compute the combined partial currents during each outer iteration, and Eqs. (19) and (20) are used to compute the flux moments. When these latter equations are written for the adjoint flux moments in terms of the combined partial currents, we obtain

$$\begin{bmatrix} \phi_{gh}^* \\ \phi_{gz}^* \end{bmatrix} = \begin{bmatrix} S_g^{-1} Q_{gh}^* \\ S_{gz}^{-1} Q_{gz}^* \end{bmatrix} + \begin{bmatrix} (S_g \nu)^{-1} & 0 \\ 0 & (S_{gz} \nu_z)^{-1} \end{bmatrix} \begin{bmatrix} B_g^T & N_g^T \\ 0 & M_g^T \end{bmatrix} (\hat{C}_g^T)^{-1} \begin{bmatrix} K_{gh}^{o*} \\ K_{gz}^{o*} \end{bmatrix} . \tag{44}$$

The formulation of Eqs. (41) and (44) permits their solution using essentially the same inner and outer iteration strategy employed for the forward solution in DIF3D-nodal. Although the asymptotic source extrapolation scheme used to accelerate the outer iterations could be retained, the existing coarse mesh rebalance (CMR) scheme had to be bypassed because the flux moment equation (Eq. (44)) depends only on the outgoing partial currents and not on the incoming partial currents. Alternatives to the CMR acceleration scheme are currently being explored for the mathematical adjoint calculation.

Following the convergence of the adjoint solution, the adjoint outgoing partial currents at internal interfaces are recovered from the combined partial currents by using Eq. (38), i.e.

$$\begin{bmatrix} J^{o*}_{gh} \\ J^{o*}_{gz} \end{bmatrix} = \begin{bmatrix} \boldsymbol{n}^{-1} & 0 \\ 0 & \boldsymbol{n}_z^{-1} \end{bmatrix} (\hat{\boldsymbol{C}}^T_g)^{-1} \begin{bmatrix} K^{o*}_{gh} \\ K^{o*}_{gz} \end{bmatrix} . \tag{45}$$

Once the adjoint fluxes and outgoing partial currents have been determined, the adjoint incoming partial currents can be obtained from Eqs. (23) and (24) via

$$J^{in*}_{gh} = \boldsymbol{n}^{-1} [\boldsymbol{Y}^T_g \boldsymbol{\nu} \phi^*_{gh} + \boldsymbol{H}^T_g \boldsymbol{\nu}_z \phi^*_{gz} + \boldsymbol{C}^T_g \boldsymbol{n} J^{o*}_{gh}] , \tag{46}$$

$$J^{in*}_{gz} = \boldsymbol{n}_z^{-1} [\boldsymbol{W}^T_g \boldsymbol{\nu} \phi^*_{gh} + \boldsymbol{V}^T_g \boldsymbol{\nu}_z \phi^*_{gz} + \boldsymbol{F}^T_g \boldsymbol{n}_z J^{o*}_{gz}] . \tag{47}$$

NUMERICAL RESULTS

The solution method presented above has been verified by demonstrating that calculated results match those obtained with the existing similarity transformation approach for problems in which that approach is exact. For example, the new solution scheme was shown to produce the same eigenvalues and mathematical adjoint flux moments and partial currents as the existing approach for several two-dimensional test cases, as well as for degenerate three-dimensional cases (axially uniform problems modeled with zero net current conditions at axial boundaries). Some three-dimensional test cases for which the existing similarity transformation scheme provided very accurate results have also been analyzed, specifically problems in which the flat transverse-leakage approximation is adequate. The results obtained for these problems verified conclusively that the direct solution method indeed produces the exact mathematical adjoint solution.

The availability of the new adjoint solution scheme provides a convenient means for determining the adequacy of the existing approximate mathematical adjoint solution scheme. Of particular interest are the perturbation theory results (obtained here with the VARI3D code[9]) using the computed adjoint solution.

The 600 MWe, low sodium-void-worth liquid metal reactor (LMR)[10] design shown in Fig. 1 was used to test the accuracy of the existing mathematical adjoint scheme. This design employs a "pancaked", annular core geometry, with an active core height of 45 cm and a four-row non-fueled central region. Axially, the active core is surrounded by a lower reflector region and an upper plenum region. The core is surrounded radially by one row of steel reflector assemblies, followed by two rows of shield assemblies. Sodium void reactivity results for this reactor design are presented in Table 1. These results can be summarized as follows:

(1) The exact reactivity values (determined by eigenvalue difference) are reproduced when the new adjoint solution flux moments and partial currents are used in exact perturbation theory calculations.

(2) For this reactor configuration, in which the quadratic transverse leakage approximation is

more accurate than the flat leakage approximation, the physical adjoint eigenvalue differs noticeably from the mathematical adjoint eigenvalue, with the difference increasing with axial mesh size.

(3) Although the existing approximate mathematical adjoint method (which employs a similarity matrix transformation in obtaining the mathematical adjoint solution from the physical adjoint fluxes) is only rigorous in the limit of zero axial mesh size when the quadratic transverse leakage approximation is used, the differences between reactivity values computed with the existing and new mathematical adjoint solutions are negligible even when conventional axial mesh spacings (approximately 15-20 cm in the active core) are employed.

Table 2 contains a summary of the groupwise maximum errors in the adjoint nodal quantities determined with the existing scheme for the unperturbed state of the above LMR model. The nodal calculation employs axial node sizes of 15.0, 14.3, and 15.0 cm in the active core, top plenum, and bottom reflector, respectively. Table 2 excludes errors in very small adjoint quantities, specifically those less than 1 % of the largest adjoint node-average flux for each group. The maximum errors in the adjoint node-averaged fluxes (zeroth flux moments) and hex-plane partial currents occur primarily in the upper plenum region, while the maximum errors in the flux moments and Z-direction adjoint partial currents occur in the upper plenum region or on nodal interfaces with control assemblies. As shown in Table 2, the maximum errors in the node-averaged fluxes are consistently lower than those in the other flux moments and partial currents. This fact, together with the location of the errors, accounts for the remarkable accuracy of the reactivity values obtained using the existing, approximate scheme for computing the adjoint. However, the rigor of the new, direct adjoint scheme is likely to be of practical importance in certain applications (e.g. generalized perturbation theory[11] for local response functionals) requiring accurate local predictions of adjoint flux moments and partial currents.

SUMMARY

A new, direct scheme has been developed for rigorously computing the mathematical adjoint for the DIF3D-nodal equations in hexagonal-Z geometry. The unknowns in the mathematical adjoint equations were redefined in a way that permitted the application of the same basic algorithm currently in use for computing the real flux, with only minor changes to the DIF3D-nodal code being required.

Differences between the local or global reactivities computed with the direct mathematical adjoint scheme and the existing approximate scheme (based on a similarity transformation) were found to be small. However, larger differences were observed in the mathematical adjoint flux moments and partial currents, and thus more significant differences may be obtained in future generalized perturbation theory applications, where localized responses are often of interest.

REFERENCES

1. R. D. Lawrence, "Perturbation Theory Within the Framework of a Higher Order Nodal Method," *Trans. Am. Nucl. Soc.*, **46**, 402 (1984).

2. T. A. Taiwo and A. F. Henry, "Perturbation Theory Based on a Nodal Model," *Nucl. Sci. Eng.*, **92**, 34 (1986).

3. P. Kao and A. F. Henry, "Supernodal Analysis of PWR Transients," *Proceedings of the Topical Meeting on Advances in Nuclear Engineering Computation and Radiation Shielding*, Santa Fe, New Mexico, p. 63, Vol. 2, American Nuclear Society, April 1989.

4. T. A. Taiwo and H. S. Khalil, "An Improved Quasistatic Option for the DIF3D Nodal Kinetics Code," *Proceedings of the Topical Meeting on Advances in Reactor Physics*, Charleston, South Carolina, p. 2-469, March 1992.

5. T. A. Taiwo, "Mathematical Adjoint Solution to the Nodal Code QUANDRY," *Trans. Am. Nucl. Soc.*, **55**, 580 (1987).

6. R. D. Lawrence, "The DIF3D Nodal Neutronics Option for Two- and Three-Dimensional Diffusion Theory Calculations in Hexagonal Geometry," ANL-83-1, Argonne National Laboratory, March 1983.

7. W. S. Yang, "Similarity Transformation Procedure for Nodal Adjoint Calculations." *Trans. Am. Nucl. Soc.*, **66**, 270 (1992).

8. K. L. Derstine, "DIF3D: A Code to Solve One-, Two-, and Three-Dimensional Finite Difference Diffusion Theory Problems," ANL-82-64, Argonne National Laboratory, April 1984.

9. P. J. Finck, private communication, Argonne National Laboratory, June 1992.

10. Y. I. Chang, et al., "Core Concepts for Zero-Sodium-Void-Worth Core in Metal Fuelled Fast Reactors," *Proc. Intl. Conf. on Fast Reactors and Related Fuel Cycles*, Kyoto, Japan, October 1991.

11. M. L. Williams, "Perturbation Theory For Nuclear Reactor Analysis," *CRC Handbook of Nuclear Reactors Calculations*, Vol. III, p. 63, CRC Press, Inc. 1986.

Table 1. Comparison of Perturbation Results Obtained with the New and Existing Adjoint Schemes for a LMR Test Case

	Existing Approximate Scheme			New Solution Scheme		
	Mesh 1	Mesh 2	Mesh 3	Mesh 1	Mesh 2	Mesh 3
Axial Mesh, cm						
Active Core	9.0	15.0	22.5	9.0	15.0	22.5
Top Plenum	9.1	14.3	33.3	9.1	14.3	33.3
Bottom Reflector	9.0	15.0	30.0	9.0	15.0	30.0
Unperturbed k-eff	1.0145319	1.0149454	1.0172300	1.0145319	1.0149454	1.0172300
Unperturbed k-eff (Adjoint)[a]	-	1.0148294	-	1.0145319	1.0149454	1.0172300
Sodium Void Reactivity, 100% Voiding[b] - Exact Perturbation Theory						
Perturbed k-eff (Adjoint)[a]	1.0180597	1.0183938	1.0199742	1.0180920	1.0184963	1.0205010
Reactivity	3.456E-03	3.455E-03	3.136E-03	3.447E-03	3.435E-03	3.151E-03
Sodium Void Reactivity, 2% Voiding[b] - Exact Perturbation Theory						
Perturbed k-eff (Adjoint)[a]	1.0145948	1.0149292	1.0167545	1.0146319	1.0150451	1.0173243
Reactivity	9.716E-05	9.698E-05	9.049E-05	9.706E-05	9.673E-05	9.169E-05
Sodium Void Reactivity, 2% Voiding[b] - First Order Perturbation Theory						
Reactivity						
Total	-	9.627E-05	-	-	9.599E-05	-
Core	-	2.083E-04	-	-	2.086E-04	-
Plenum	-	-1.120E-04	-	-	-1.126E-04	-
Node 1[c]	-	7.097E-06	-	-	7.089E-06	-
Node 2[c]	-	-2.028E-07	-	-	-2.035E-07	-

[a]For the existing scheme this is the k-eff of the physical adjoint solution, whereas in the new scheme it is the k-eff of the mathematical adjoint solution.

[b]100% voiding denotes complete voiding of flowing sodium.

[c]Nodes 1 and 2 are individual nodes in the core and plenum, respectively.

Table 2. Errors in Adjoint Solution Computed with the Existing Scheme

Energy Group	Maximum Errors in Adjoint Nodal Quantities[a] (%)				
	Average Flux	Flux Moments		Partial Currents	
		Hex-plane	Z-direction	Hex-plane	Z-direction
1	0.87	7.79	12.18	69.19	86.27
2	0.82	8.45	10.10	55.52	75.11
3	0.87	8.31	9.51	42.49	82.99
4	0.93	8.30	9.26	58.65	75.79
5	0.94	6.29	6.47	41.64	64.05
6	1.07	5.10	6.84	32.76	53.96
7	1.36	6.48	11.80	28.69	55.56
8	1.42	5.59	16.53	25.41	61.20
9	1.60	5.60	21.06	37.59	65.51
10	1.39	5.25	26.86	32.93	71.06
11	1.15	5.32	32.43	40.38	75.65
12	1.41	5.90	40.29	50.50	76.66
13	1.39	4.98	42.56	45.01	78.62
14	1.66	6.07	53.01	39.58	81.89
15	3.47	8.05	62.66	32.74	37.83
16	4.26	8.32	63.71	29.93	37.12
17	2.52	5.92	23.23	28.85	38.65
18	2.45	6.21	70.87	28.38	43.24
19	2.43	11.11	26.25	23.66	49.44
20	2.52	11.09	31.15	49.26	52.37
21	7.31	16.34	73.42	89.40	64.86

[a]Only quantities exceeding 1 % of the largest adjoint node-average flux are considered for each group.

Figure 1. Low Sodium-Void-Worth LMR Core Layout

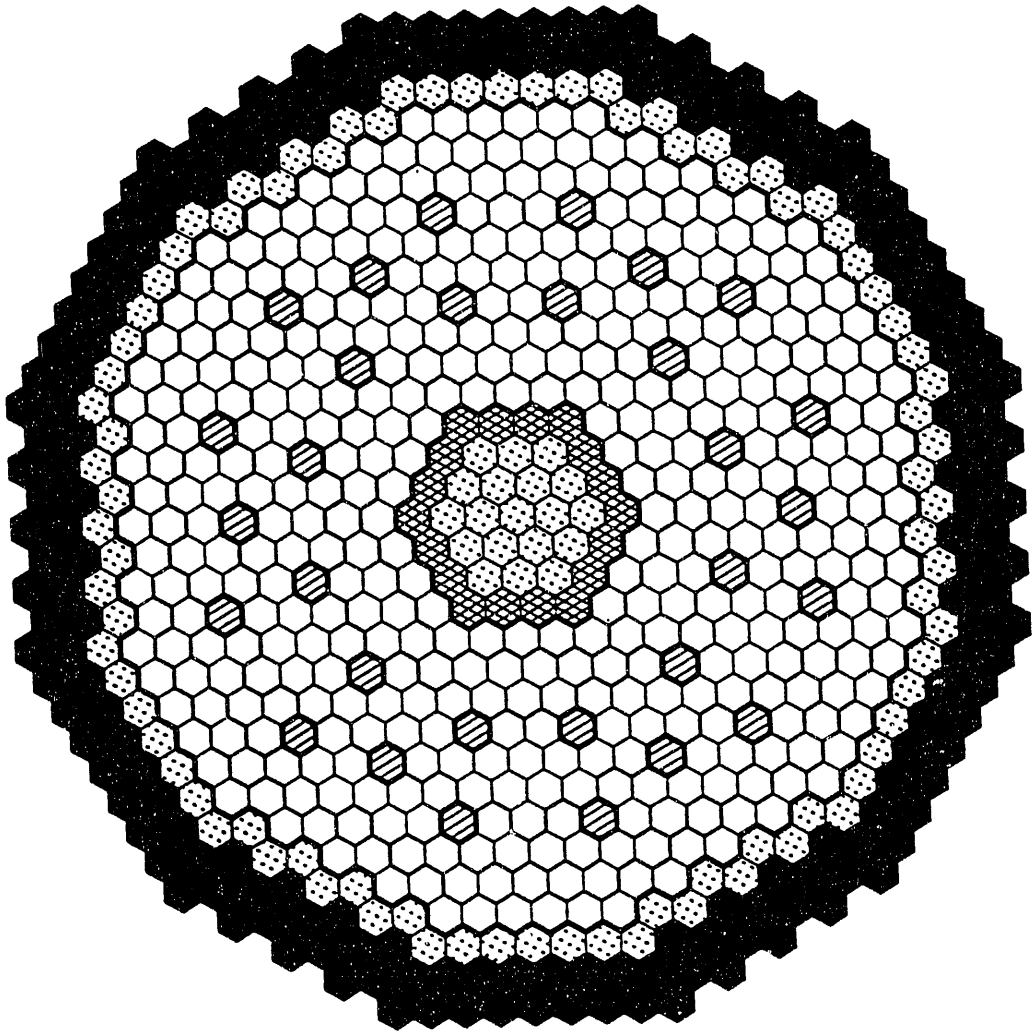

DRIVER ASSEMBLY (420)

STEEL REFLECTOR (103)

CONTROL ASSEMBLY (30)

SHIELD ASSEMBLY (186)

B4C EXCHANGE ASSEMBLY (18)

END

DATE
FILMED
6/17/93